



Brief Communications

Measuring the soot onset temperature in high-pressure *n*-dodecane spray pyrolysis

Scott A. Skeen*, Koji Yasutomi

Combustion Research Facility, Sandia National Laboratories, 7011 East Ave., Livermore, CA 94550, United States

ARTICLE INFO

Article history:

Received 19 April 2017

Revised 5 June 2017

Accepted 21 September 2017

Keywords:

Soot

Pyrolysis

High-speed imaging

Spray combustion

ABSTRACT

Soot formation in pyrolyzing sprays of *n*-dodecane is visualized and quantified in a high-pressure, high-temperature, constant-volume spray chamber at 38 bar, 76 bar, and 114 bar. Sprays of *n*-dodecane are injected at 500 bar from a single-hole, 186- μ m orifice diameter fuel injector. We quantify the temporal evolution of the soot optical thickness and the total soot mass formed in the pyrolyzing sprays using a high-speed extinction imaging diagnostic. The vessel ambient temperature and pressure are varied independently to identify the soot onset temperature for *n*-dodecane pyrolysis. Linear extrapolation of the maximum soot formation rates as a function of ambient temperature reveals a soot onset temperature near 1450 K. The onset temperature determined here for *n*-dodecane is within 50 K of those previously measured along the centerline of atmospheric pressure coflow diffusion flames for smaller alkane fuels.

© 2017 The Combustion Institute. Published by Elsevier Inc. All rights reserved.

1. Introduction

Laminar flame studies conducted at atmospheric pressure by Gomez et al. [1] and Saito et al. [2] revealed a relatively consistent soot onset temperature between 1310 K and 1400 K for a variety of hydrocarbon fuels. To determine the onset temperature, the authors used a fine-wire thermocouple and measured the temperature along the flame centerline until soot deposits were observed. The radiation corrected temperature at the highest centerline axial location prior to soot deposition defined the onset temperature. For clarity, we mention that the onset temperature as it is defined and used in the present work differs from the soot “inception” temperature near 1600 K (or higher) reported in [3–8]. Whereas, the onset temperature measured in [1,2] was determined in a region where oxidation is not expected to inhibit soot formation, studies referencing the inception temperature have generally been conducted under conditions where competition between soot formation and oxidation occurs.

Of the 12 flames studied in Gomez et al. [1], all were established at the smoke height condition with the exception of one of the butene flames. Saito et al. [2] selected small diffusion flames for their study since such flames remain in the early stage of soot formation. For all cases in Gomez et al. [1], the soot onset location was observed at a height in the flame between 25% and 40% of the luminous flame height, while Saito et al. [2] reported that the first

soot deposits onto their probe occurred between 2 mm and 4 mm below the first visible appearance of yellow emission. Recognizing that the centerline in the near-burner region of a non-lifted coflow diffusion flame is oxygen deficient [9], these early soot processes are more representative of a pyrolysis pathway. As such, the soot onset temperatures measured by Gomez et al. [1] and Saito et al. [2] provide a suitable reference for the study of soot onset limits under pyrolytic conditions or conditions expected to have very small quantities of oxidizing species.

In addition to diffusion flame studies, shock tubes have been widely used to investigate pyrolytic soot formation processes and establish temperature dependencies for a wide range of fuels. Graham and co-workers [10] were pioneers in this area followed by the large body of work from Frenklach [11–17]. Soot yields are generally negligible in shock tube pyrolysis experiments at temperatures below 1500 K; however, with the addition of a small amount of oxygen soot has been observed during acetylene/oxygen/argon mixtures in the shock tube below 1400 K [14]. To understand the effect of oxygen on soot formation, Gülder [18] added oxygen to the fuel stream in laminar coflow flames of methane, propane, and *n*-butane. They observed that oxygen suppressed soot formation in methane flames while enhancing soot formation in propane and *n*-butane flames. Suppression of soot in methane flames was attributed to a reduction in acetylene as a pyrolysis product while the enhancement observed for propane and *n*-butane flames was related to oxygen stimulating fuel pyrolysis and the production of H atoms and other hydrocarbon radicals. Hwang et al. [19] investigated the influence of adding a small amount of oxygen to the fuel in counterflow ethylene diffusion flames and concluded that

* Corresponding author.

E-mail address: sskeen@sandia.gov (S.A. Skeen).

reactions between O atoms and acetylene enhance the formation of key soot precursor species. Oxygen's enhancement of fuel decomposition and soot precursor formation leading to increased soot in these flame studies is consistent with the reduced soot onset temperature in shock tube studies when a small amount of oxygen was included in the mixture.

This brief communication presents measurements of the soot onset temperature in pyrolyzing sprays of *n*-dodecane in a constant volume, high-pressure, high-temperature, pre-burn chamber. We use the term “pyrolyzing” loosely here as the pre-burn products, which consist mainly of nitrogen, also include small amounts of carbon dioxide and water. Over the range of temperatures and pressures considered (1400 K – 1750 K, 38 bar – 114 bar) ppm quantities of the hydroxyl radical (OH), hydrogen, and oxygen would be present at equilibrium. Such small quantities of OH and oxygen may promote earlier and/or more rapid fuel decomposition than a purely inert environment, but would not be sufficient to open oxidation pathways in competition with soot formation. A high-speed, diffused back-illumination extinction imaging (DBIEI) diagnostic enabled time-resolved, quantitative measurements of the total soot mass. The maximum formation rate of soot as a function of ambient temperature was derived from the time-resolved imaging extinction measurements and a linear extrapolation was performed to determine the soot onset temperature. We observed a soot onset temperature near 1450 K for the pyrolyzing *n*-dodecane sprays, which is within 50 K of the onset temperatures measured for smaller alkanes in atmospheric pressure, coflow diffusion flames [2].

2. Experimental

2.1. Combustion vessel and injection system

Sprays of *n*-dodecane were injected into the optically accessible, high-pressure, constant-volume combustion vessel depicted in Fig. 1. The combustion chamber is nearly cubical with a characteristic dimension of 108 mm. Six round ports of 105-mm diameter constitute the four sides and top and bottom of the chamber with eight 19-mm diameter ports located at the corners. The water-cooled fuel injector (Bosch 3-22) is mounted horizontally in one of the side ports with two spark plugs mounted in the top port and three fine-wire type-R thermocouples mounted in the bottom port. Sapphire windows occupy the remaining three side ports for optical access. Pneumatic intake and exhaust valves reside in two of the corner ports on the injector side of the vessel along with a pressure transducer (Kistler K-6001). The fourth corner port on the injector side is unused. A second pressure transducer, a sheathed

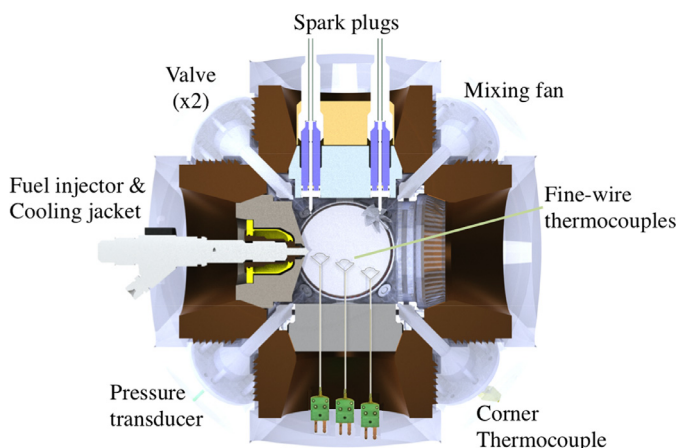


Fig. 1. Schematic cross-section of constant volume pre-burn vessel.

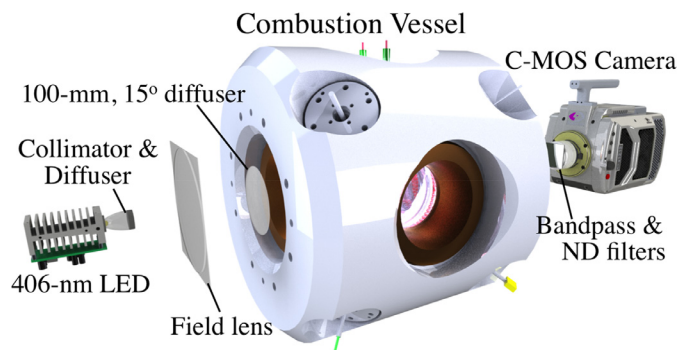


Fig. 2. Diagram of the high-pressure combustion vessel and diffused back-illumination extinction imaging (DBIEI) optical arrangement.

type-J thermocouple, and the mixing fan occupy three of the four corner ports on the opposite side of the injector port with the fourth corner port on this side also unused.

The temperatures and pressures desired for this study were achieved via the combustion of a spark-ignited premixed charge. The premixed charge gases include acetylene, hydrogen, nitrogen, and oxygen and batches of the desired mixture are prepared manometrically and stored external to the laboratory prior to the experiments. Following the aforementioned “pre-burn” event, a cool-down period ensues resulting in a time-dependent range of thermodynamic conditions into which the fuel spray can be injected. The present work employed a stoichiometric pre-burn charge resulting in an ambient environment containing 89.71% nitrogen, 6.52% carbon dioxide, and 3.77% water by volume. The conditions therefore do not represent pyrolysis in the purest sense since ppm levels of OH and O₂ are expected based on equilibrium calculations at temperatures exceeding 1400 K.

Target ambient conditions ranged from 1400 K to 1700 K (50 K steps) at pressures of 38 bar, 76 bar, and 114 bar. Temperature measurements at three axial locations within a few millimeters of the penetrating fuel vapor/soot boundary were acquired using the thermocouples mounted in the bottom vessel port. Radiation corrections were performed and uncertainty in the temperature measurements is estimated to be ± 25 K.

A syringe pump (Teledyne 30D) pressurizes the fuel to 500 bar prior to injection and the injector has a single axial orifice with a 186- μ m nominal diameter. We targeted short injection durations (120 μ s) and a relatively low common-rail injection pressure to limit vapor penetration and the mass of fuel injected. By limiting vapor penetration, the conversion of fuel vapor to soot can be imaged over a longer period of time while the entire spray remains within the field of view of the imaging system described in the next section.

2.2. Diffused back-illumination extinction imaging (DBIEI)

We quantified soot formation following pyrolytic decomposition of *n*-dodecane using the high-speed imaging extinction diagnostic illustrated in Fig. 2. The main components of this diagnostic include a high-output, ultra-fast, deep blue (406-nm, 17-nm FWHM) light emitting diode (LED) equipped with a collimator, two engineered diffusers, a field lens, and a high-speed camera. The first engineered diffuser (25-mm diameter, circular 50-degree distribution) was mounted at the exit of the LED collimator. The light passing through this first diffuser was collected by the 150-mm diameter, 150-mm focal length field lens. The field lens directed the nearly collimated light to the second diffuser, which has a 100-mm diameter and a circular 15-degree distribution. The high speed camera was operated at 50,000 frames per second and was

equipped with a 50-mm f/1.2 Nikkor lens, a 500D close-up lens, a 400-nm (25-nm FWHM) band-pass filter, and an OD 1.5 neutral density filter. The light source setup described above directs the diffused illumination toward the spray plane with a quasi-Lambertian distribution, resulting in minimal light extinction induced by refractive index gradients (i.e., beam steering). A detailed description of the DBIEI diagnostic is available in Westlye et al. [20].

Pulsing the LED in every other camera frame enables the removal of sensor background signal and broadband emission from hot soot particles at each time step. The background corrected 2-D extinction measurements were converted to optical thickness, KL , using the well-known Beer-Lambert law.

$$I/I_0 = \exp(-KL). \quad (1)$$

In Eq. (1), I is the transmitted LED intensity, I_0 is the incident intensity, K is the dimensional extinction coefficient, and L is the path length through the soot cloud. Because the total soot mass (m_{soot}) is proportional to the observed optical thickness (KL), one can derive the soot mass within each pixel according to Eq. (2). The total soot mass is then the sum of all pixel specific values over the entire image.

$$m_{\text{soot, pixel}} = \frac{\lambda \cdot \rho_{\text{soot}}}{k_e} KL \cdot \Delta A_{\text{pixel}} \quad (2)$$

In Eq. (2), λ is the wavelength of incident light, k_e is the non-dimensional extinction coefficient, ρ_{soot} is the soot mass density, and ΔA is the projected pixel area.

Williams et al. [21] measured values for k_e ranging from approximately $k_e = 6$ to $k_e = 10$ for a number of fuels and burner configurations at an incident wavelength of 635 nm. Minimal dependence on height above burner was observed, suggesting that k_e

was not a strong function of soot maturity in their study. In the present work, we used $k_e = 8$ after considering that soot formed under pyrolysis may have a smaller scattering albedo thereby lowering k_e , while the shorter wavelength of incident light is expected to result in a higher k_e . The soot mass density (ρ_{soot}) was assumed to be 1.8 g/cm^3 [22], although Totten et al. [23] suggested that nascent soot may have a mass density near 1.12 g/cm^3 . Uncertainty in our results associated with these assumptions will be discussed below.

3. Results and discussion

False-color KL maps showing the time evolution of the imaged optical thickness in three pyrolyzing sprays at the 76 bar/1500 K ambient condition appear in Fig. 3. The top frames show extinction due to the liquid fuel injection and extinction in the subsequent frames is attributed to soot. The three independent injection events show consistency in the timing at which extinction of the incident light by soot is first observed ($\sim 0.84 \text{ ms}$). For all cases with ambient temperatures of 1500 K and above, similar consistency was observed. For the 1400 K and 1450 K cases, shot-to-shot variability increased presumably due to local temperature fluctuations below and above the apparent soot onset limit temperature.

Figure 4 provides the time-resolved total soot mass at 76 bar for each of the ambient temperature conditions considered. For all cases, soot mass density and the non-dimensional extinction coefficient were assumed invariant with time, pressure, and temperature—the implications of which are discussed below. The line plots represent the ensemble average of the repeated runs and the shaded region indicates \pm one standard deviation ($\pm\sigma$). The S-shaped character of the total soot mass is representative of an autocatalytic process and is consistent with the soot yield

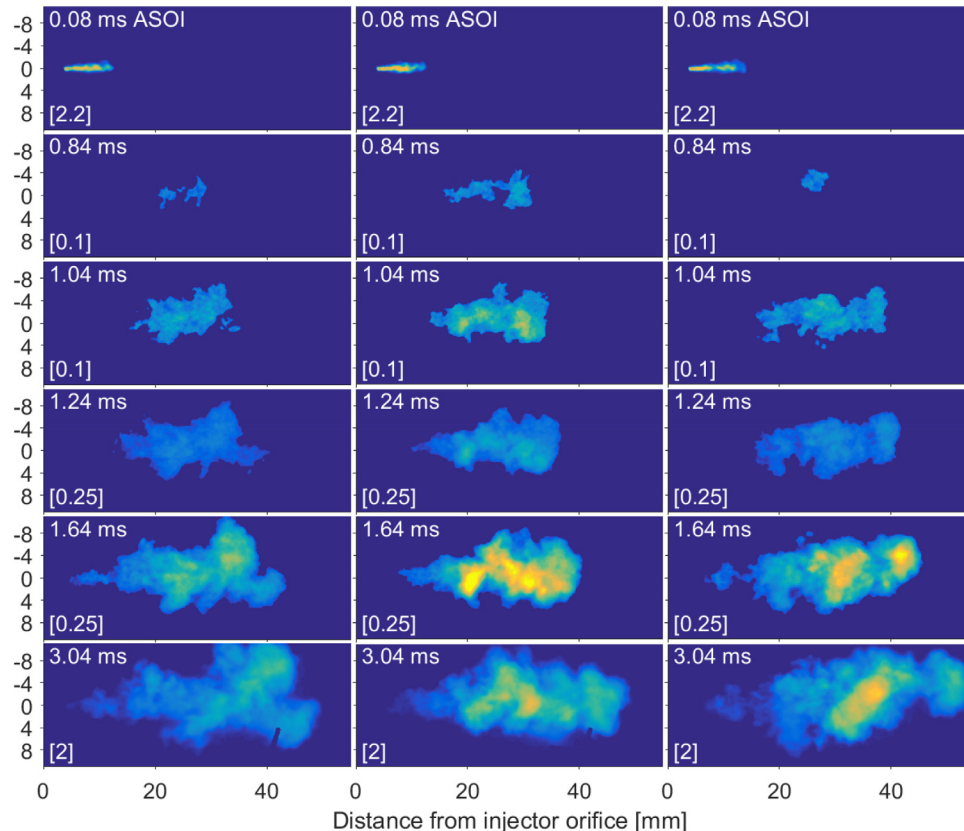


Fig. 3. False-color maps of the imaged light extinction during pyrolysis of *n*-dodecane at 1500 K and 76 bar. The time after the start of injection (ASOI) is provided in the upper left corner of each frame. The bracketed value in the lower left corner indicates the maximum value of the false-color scale representing the magnitude of KL .

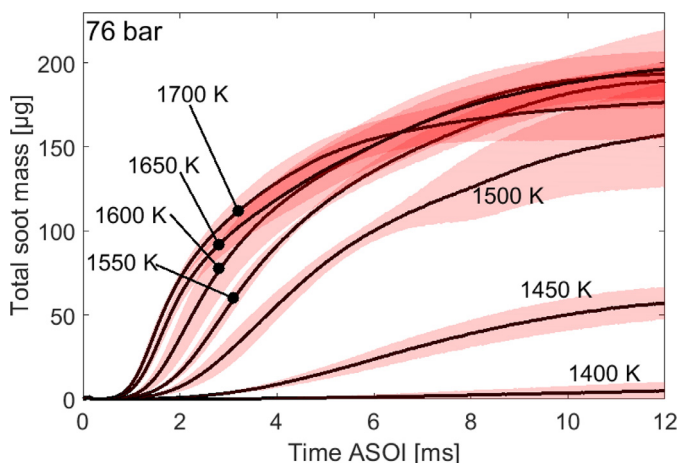


Fig. 4. Total soot mass as a function of time ASOI for seven different ambient temperature conditions at an ambient pressure of 76 bar. The data have been ensemble averaged over multiple repeated events having the same target ambient conditions. The shaded regions represent $\pm \sigma$.

curves observed in a shock tube by Frenklach et al. [16,17]. To determine the maximum soot formation rate for each individual run, we fit a third order polynomial to the region containing the maximum slope and computed the derivative. We observe an increase in the maximum rate of soot formation with increasing temperature; however, the peak total soot mass is consistent for all cases (including those at 38 bar and 114 bar) at 1550 K and above. Thus, for the conditions of the present study, 1550 K appears to be a critical temperature above which additional soot yields are not observed.

Uncertainty in quantifying the total soot mass arises mainly from assumptions about the soot mass density (ρ_{soot}) and non-dimensional extinction coefficient (k_e) (see Eq. (2)). Based on the work of Williams et al. [21], one might assume $7 < k_e < 11$ after accounting for the effect of the shorter incident light wavelength used in the present study. As the total soot mass scales linearly with k_e , this range of possible values alone could result in error as large as 60%. Error due to uncertainty in ρ_{soot} , with values ranging from 1.12–1.8 g/cm³ [23], is equally as large. Nevertheless, one can argue that these errors may have a compensating effect given that light extinction by lower mass density soot may be dominated by absorption leading to smaller k_e values, while higher mass density soot may have a significant scattering contribution leading to larger k_e values [21]. This same argument can be applied when considering errors associated with the assumption of a time- and temperature-invariant k_e throughout the soot formation and growth processes in these pyrolyzing sprays. That is, the first soot formed in the pyrolyzing spray or soot formed at lower temperature conditions may be less graphitic and therefore characterized by a lower mass density and smaller k_e value. As time progresses or higher temperature conditions are considered, the particles have time or temperature for further dehydrogenization, growth, and agglomeration leading to higher mass densities, increased scattering albedo, and larger k_e . At present, we cannot speculate on the effect ambient pressure might have on ρ_{soot} or k_e .

Based on the carbon available in the total injected fuel and assuming an atomic carbon-to-hydrogen ratio of C/H = 8 [24,25], approximately 33%, 50%, and 70% of the fuel carbon is converted to soot at 38 bar, 76 bar, and 114 bar, respectively. Without a direct measurement of the carbon-to-hydrogen ratio for the particles formed in these pyrolyzing sprays, there is some uncertainty in the carbon conversion numbers presented above. Dobbins et al.

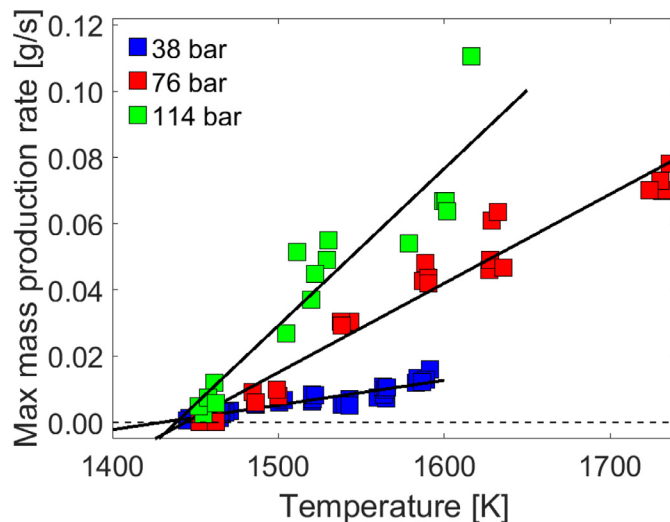


Fig. 5. Maximum rate of soot formation as a function of ambient temperature for three different ambient pressure conditions.

reported an atomic carbon-to-hydrogen ratio as low as C/H = 1.75 for soot “precursor particles” sampled from the centerline of an ethylene coflow diffusion flame 20 mm above the burner [26]. Implementing this lower C/H ratio reduces the computed fuel carbon conversion by 1–3 percentage points. With regard to the incontrovertible increase in soot yield observed at higher ambient pressures, further work will be required to understand the effects of enhanced mixing and/or soot kinetics.

In Fig. 5, the maximum soot formation rate for each run is plotted against the corresponding ambient temperature in a scatter plot. The linear fit applied to data from each ambient pressure condition is extrapolated through zero to determine the soot onset temperature, which is observed near 1450 K \pm 25 K. Saito et al. [2] reported soot onset temperatures for methane and ethane of 1390 K \pm 20 K and 1399 K \pm 20 K, respectively, along the centerline of atmospheric pressure, coflow diffusion flames. Lower soot onset temperatures were observed for allene (1310 K), 1,3-butadiene (1350 K), and acetylene (1350 K). In retrospect, these lower onset temperatures may be due to lower kinetic barriers in the formation of the resonantly stabilized propargyl radical—believed to be a critical step in the formation of the first aromatic ring and subsequent aromatic growth leading to soot particle inception for aliphatic fuels [27,28]. As discussed previously, Frenklach [14] observed soot formation at temperatures below 1400 K in a shock tube for acetylene and argon mixtures when a small amount of oxygen was added, whereas pure pyrolysis experiments typically require temperatures exceeding 1600 K. Thus, there is evidence that small quantities of oxygen containing radical species must be available to promote fuel decomposition in the present work as well as along the centerline of the coflow flame experiments of Gomez et al. [1] and Saito et al. [2].

We also note that Herbinet et al. [29] found the dominant products of *n*-dodecane decomposition to include the alkenes 1-butene, 1,3-butadiene, ethylene, and propene; however, considering that the alkene fuels studied in Saito et al. [2] demonstrated soot onset temperatures at 1350 K and below, it seems the chemical structure of the parent fuel rather than its decomposition products may govern the kinetics related to soot onset under the conditions of the present study.

Finally, we point out that the large uncertainties in soot density and non-dimensional extinction coefficient discussed previously should have a reduced impact on the determination of the soot onset temperature for the following two reasons. First, the

maximum formation rate corresponds to data within a short time window where significant changes to soot characteristics would not be expected. Second, assuming that the soot characteristics are consistent among the different temperature conditions during the period of maximum increase in total soot mass, the use of a more accurate soot mass density and/or non-dimensional extinction coefficient would scale the data linearly resulting in the same intercept with the abscissa.

4. Summary and conclusions

This brief communication presents time-resolved measurements of soot formation in high-pressure pyrolyzing sprays of *n*-dodecane in a constant volume pre-burn vessel. The soot optical thickness and corresponding total soot mass were measured by diffused back illumination extinction imaging (DBIEI). Consistent with previous shock tube studies, the time-resolved soot yield was characterized by an S-type curve indicative of an autocatalytic process. A critical temperature of 1550 K was observed, above which the ultimate conversion of fuel carbon to soot did not increase with increasing ambient temperature. The maximum rate of soot formation increased linearly with increasing ambient temperature at constant pressure. Linear fits to the peak rate of soot formation as a function of ambient temperature intercept the x-axis near 1450 K thereby identifying a pressure invariant soot onset temperature for *n*-dodecane. The soot onset temperature reported here is within 50 K of values reported for smaller alkanes (CH_4 , C_2H_6) in atmospheric pressure coflow diffusion flame studies.

Acknowledgments

The experiments were conducted at the Combustion Research Facility, Sandia National Laboratories, Livermore, CA. Support for this work was provided by Sandia National Laboratories under the Laboratory-Directed Research and Development (LDRD) program. Sandia National Laboratories is a multi-mission laboratory managed and operated by National Technology and Engineering Solutions of Sandia, LLC, a wholly owned subsidiary of Honeywell International, Inc., for the U.S. Department of Energy's National Nuclear Security Administration under contract [DE-NA0003525](#). Chris Carlen, Dave Ciccone, and Aaron Czeszynski are gratefully acknowledged for technical assistance. The authors also wish to thank Gurpreet Singh and Leo Breton, program managers at U.S. DOE, for their support.

References

- [1] A. Gomez, M. Littman, I. Glassman, Comparative study of soot formation on the centerline of axisymmetric laminar diffusion flames: Fuel and temperature effects, *Combust. Flame* 70 (1987) 225–241.
- [2] K. Saito, A. Gordon, F. Williams, W. Stickle, A study of the early history of soot formation in various hydrocarbon diffusion flames, *Combust. Sci. Technol.* 80 (1991) 103–119.
- [3] K.T. Kang, J.Y. Hwang, S.H. Chung, W. Lee, Soot zone structure and sooting limit in diffusion flames: Comparison of counterflow and co-flow flames, *Combust. Flame* 109 (1997) 266–281.
- [4] B. Kumfer, S. Skeen, R. Chen, R. Axelbaum, Measurement and analysis of soot inception limits of oxygen-enriched coflow flames, *Combust. Flame* 147 (2006) 233–242.
- [5] B. Kumfer, S. Skeen, R. Axelbaum, Soot inception limits in laminar diffusion flames with application to oxy-fuel combustion, *Combust. Flame* 154 (2008) 546–556.
- [6] I. Glassman, O. Nishida, G. Sidebotham, Critical temperatures of soot formation, in: H. Bockhorn (Ed.), *Soot Formation in Combustion*, Springer-Verlag, New York, 1994, pp. 316–324.
- [7] C.S. McEnally, L.D. Pfefferle, Flow time effects on hydrocarbon growth and soot formation in coflowing methane/air non-premixed flames, *Symp. (Int.) Combust.* 27 (1998) 1539–1547.
- [8] C.S. McEnally, L.D. Pfefferle, Comparison of non-fuel hydrocarbon concentrations measured in coflowing nonpremixed flames fueled with small hydrocarbons, *Combust. Flame* 117 (1999) 362–372.
- [9] I.M. Kennedy, C. Yam, D.C. Rapp, R.J. Santoro, Modeling and measurements of soot and species in a laminar diffusion flame, *Combust. Flame* 107 (1996) 368–382.
- [10] S.C. Graham, J.B. Homer, J.L.J. Rosenfeld, The formation and coagulation of soot aerosols generated by the pyrolysis of aromatic hydrocarbons, *Proc. R. Soc. Lond. A Mat.* 344 (1975) 259–285.
- [11] M. Frenklach, D.W. Clary, W.C. Gardiner, S.E. Stein, Detailed kinetic modeling of soot formation in shock-tube pyrolysis of acetylene, *Symp. (Int.) Combust.* 20 (1985) 887–901.
- [12] M. Frenklach, D.W. Clary, W.C. Gardiner, S.E. Stein, Effect of fuel structure on pathways to soot, *Symp. (Int.) Combust.* 21 (1988) 1067–1076.
- [13] M. Frenklach, J. Hsu, D. Miller, R. Matula, Shock-tube pyrolysis of chlorinated hydrocarbons: Formation of soot, *Combust. Flame* 64 (1986) 141–155.
- [14] M. Frenklach, M. Ramachandra, R. Matula, Soot formation in shock-tube oxidation of hydrocarbons, *Symp. (Int.) Combust.* 20 (1985) 871–878.
- [15] M. Frenklach, S. Taki, C.L.K. Cheong, R. Matula, Soot particle size and soot yield in shock tube studies, *Combust. Flame* 51 (1983) 37–43.
- [16] M. Frenklach, S. Taki, M. Durgaprasad, R. Matula, Soot formation in shock-tube pyrolysis of acetylene, allene, and 1, 3-butadiene, *Combust. Flame* 54 (1983) 81–101.
- [17] M. Frenklach, S. Taki, R. Matula, A conceptual model for soot formation in pyrolysis of aromatic hydrocarbons, *Combust. Flame* 49 (1983) 275–282.
- [18] Ö.L. Gülder, Effects of oxygen on soot formation in methane, propane, and *n*-butane diffusion flames, *Combust. Flame* 101 (1995) 302–310.
- [19] J. Hwang, S. Chung, W. Lee, Effects of oxygen and propane addition on soot formation in counterflow ethylene flames and the role of C3 chemistry, *Symp. (Int.) Combust.* 27 (1998) 1531–1538.
- [20] F.R. Westlye, K. Penney, A. Ivarsson, L.M. Pickett, J. Manin, S.A. Skeen, Diffuse back-illumination setup for high temporally resolved extinction imaging, *Appl. Opt.* 56 (2017) 5028–5038.
- [21] T.C. Williams, C. Shaddix, K. Jensen, J. Suo-Anttila, Measurement of the dimensionless extinction coefficient of soot within laminar diffusion flames, *Int. J. Heat Mass Transf.* 50 (2007) 1616–1630.
- [22] M. Choi, G.W. Mulholland, A. Hamins, T. Kashiwagi, Comparisons of the soot volume fraction using gravimetric and light extinction techniques, *Combust. Flame* 102 (1995) 161–169.
- [23] T.S. Totton, D. Chakrabarti, A.J. Misquitta, M. Sander, D.J. Wales, M. Kraft, Modelling the internal structure of nascent soot particles, *Combust. Flame* 157 (2010) 909–914.
- [24] H.B. Palmer, C.F. Cullis, The formation of carbon from gases, *Chem. Phys. Carbon* 1 (1965) 265–325.
- [25] H.F. Calcutt, Mechanisms of soot nucleation in flames—A critical review, *Combust. Flame* 42 (1981) 215–242.
- [26] R. Dobbins, R.A. Fletcher, H.-C. Chang, The evolution of soot precursor particles in a diffusion flame, *Combust. Flame* 115 (1998) 285–298.
- [27] N. Hansen, T. Kasper, B. Yang, T.A. Cool, W. Li, P.R. Westmoreland, P. Oßwald, K. Kohse-Höinghaus, Fuel-structure dependence of benzene formation processes in premixed flames fueled by C_6H_{12} isomers, *Proc. Comb. Inst.* 33 (2011) 585–592.
- [28] N. Hansen, J.A. Miller, S.J. Klippenstein, P.R. Westmoreland, K. Kohse-Höinghaus, Exploring formation pathways of aromatic compounds in laboratory-based model flames of aliphatic fuels, *Comb. Explo. Shock* 48 (2012) 508–515.
- [29] O. Herbinet, P.-M. Marquaire, F. Battin-Leclerc, R. Fournet, Thermal decomposition of *n*-dodecane: Experiments and kinetic modeling, *J. Anal. Appl. Pyrol.* 78 (2007) 419–429.